Original Article

Institution of MECHANICAL ENGINEERS
Journal of AEROSPACE ENGINEERING

Proc IMechE Part G:
J Aerospace Engineering
0(0) 1–13

DOI: 10.1177/0954410015607897
uk.sagepub.com/jaero
SAGE

Aero engine compressor fouling effects for short- and long-haul missions

Uyioghosa Igie, Mike Goiricelaya, Devaiah Nalianda and Orlando Minervino

Abstract

The impact of compressor fouling on civil aero engines unlike the industrial stationary application has not been widely investigated or available in open literature. There are questions about the impact of fouling for short- and long-haul missions comparatively, given their unique operational requirements and market. The aim of this study is to quantify the effects of different levels of fouling degradation on the fan, for two different aircraft with different two-spool engine models for their respective typical missions. Firstly, the study shows the increase in turbine entry temperature for both aircraft engines, to maintain the same level of thrust as their clean condition. The highest penalty observed is during take-off and climb, when the thrust setting is the highest. Despite take-off and climb segment being a larger proportion in the short-haul mission compared to the long-haul mission, the percentage increase in fuel burn due to fouling are similar, except in the worst case fouling level were the former is higher by 0.8% points. In addition to this, for all the cases, the additional fuel burn due to fouling and its cost is shown to be small. Likewise, the increase in turbine entry temperature for both missions at take-off are similar, except in the worst case fouling level for the short-haul mission were the turbine entry temperature is 7 K higher than the corresponding long-haul mission for the same level of degradation. The study infers that the penalty due to rise in temperature is of more concern than the additional fuel burn. Hence the blade technology (cooling and material) and engine thrust rating are key factors in determining the extent to which blade fouling would affect aero engine performance in short- and long-haul missions.

Keywords

Jet engine model, aero engine operation, compressor fouling, degradation, short-haul, long-haul

Date received: 17 October 2014; accepted: 1 September 2015

Introduction

Aero engines are susceptible to compressor fouling as shown in Figures 1 and 2, which is the deposition and accretion of airborne particles on the compressor blades.[1] Unlike the application of gas turbines (GTs) for power generation, mechanical drive applications and helicopter engines, inlet air filtrations systems are not installed on jet engines given the nature of the operation. In addition to this, jet engines operate predominantly at cruise, which can be up to 12,000 m, where the concentration of fouling particles is negligible. Alpert et al.[2] presents the vertical distribution of Saharan dust in the Eastern and Central Mediterranean, the Chad basin in the Sahara desert and within the Eastern Atlantic. In these environments, the average vertical profiles of dust in a given month shows reducing level of dust concentration with increasing altitude; however, the concentration of dust for the same altitude were different. Some factors which can increase the rate of fouling include the seasons (rainy or high humidity) and frequency of take-off and landings. The vehicle traffic levels and size of an airport can also be another factor. For example London Heathrow airport is one of the busiest international airports in the world, located close to a major and busy motorway within proximity to industrial units. In addition to this, its aircraft ground operations and frequent take-offs and landings and airport-related car traffic all increases the susceptibility to pollutants/foulants.

As the lower atmosphere is more predisposed to airborne fouling, also due to gravity, engines operated more frequently on the lower altitudes or more flight cycles such as short-haul mission (SHM) operations are likely to be more exposed to contaminants. From the knowledge gained from studies on compressor

School of Aerospace, Transport and Manufacturing (SATM), Cranfield University, UK

Corresponding author:
Uyioghosa Igie, School of Aerospace, Transport and Manufacturing, Cranfield University, College Road, Cranfield, Bedfordshire, MK43 0AL, UK.
Email: u.igie@cranfield.ac.uk

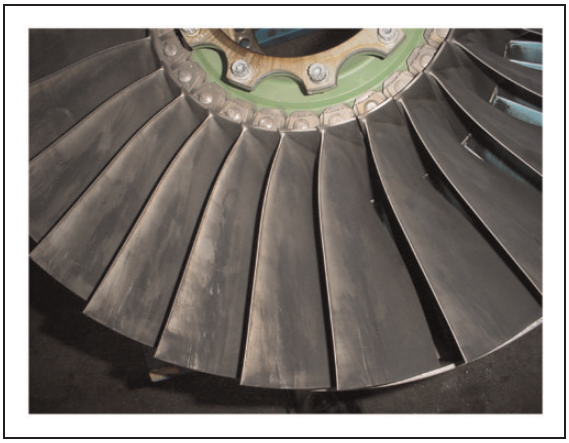

Figure 1. A fouled fan blade.

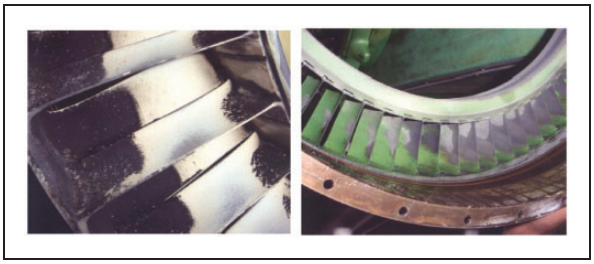

Figure 2. Fouling of low-pressure compressor stators at the front (left) and rear stage (right).

fouling for stationary applications, it is generally known that the impact includes the following:

- reduced mass flow, pressure ratio, compressor efficiency, thermal efficiency and shaft power for a given rotational speed/turbine entry temperature (TET),[1,3]
- increased fuel burn and TET to maintain the same level of shaft power[1,3] that can reduce the life of the turbine blades.

From engine flight operational data, evaluating the impact of fouling on engine performance is not simple to quantify, especially due to the changing thrust settings for different segments of the flight (take-off, cruise, descent) linked to altitude, the changing payload – even for the same mission, variation in ambient conditions, issues related to operational or certification derating of the engine and relatively limited instrumentation to enable better assessment of degradation when compared to a stationary GT for power generation. Currently, engine operational data for gas path analysis typically includes: fuel flow, the rotational speed of shafts/spools, thrust lever angle (TLA – a measure of power setting) and the interstage turbine temperature (ITT – which is the temperature between the high-pressure and low-pressure turbine). Other parameters such as the air speed, altitude and ambient conditions (temperature and pressure) that is useful in normalising data to ISA conditions to enable performance assessment is also available.

Syverud et al.[4] presents the impact of fouling, in a series of accelerated deterioration tests on a stationary General Electric J85-13 turbojet engine, using atomised saltwater droplets. This study shows that the front stages of the compressor are likely to be more fouled than the subsequent stages, as initial stages act as 'filter' to subsequent stages. This finding is consistent with many other studies including Tarabrin et al.;[5] however, these evidence are usually for stationary single-spool compressors and not cases of multiple-spools or compressors with by-pass flow. Using intake depression as a measure of mass flow through the engine, Syverud et al.[4] shows the increasing penalty on intake depression with increase in the amount of salt (6 g, 18 g and 30 g). For a given corrected rotational speed, the same amount of air flow cannot be reached with fouling. For fouling with 30 g of salt, the flow capacity at 97% corrected shaft speed is equivalent to the same amount of flow at 94% when the compressor is clean. This infers that to achieve the desired flow or thrust in fouled condition, the corrected shaft speed would need to increase. The study also points to the nonlinear shift in degraded performance, making it difficult to use just the corrected shaft speed as an indicator.

In a study that focuses more on the blade aerodynamics, Suder et al.[6] shows the impact of fouling (additional roughness and thickness) to a transonic axial compressor. A coating of 0.025 mm was applied on the suction and pressure side of the rotor blades, which led to 10% increase in thickness of the leading edge and hub, and 20% at the tip. These effects accounted for 9% decrease in pressure ratio and 6% point loss in efficiency, when operating close to design point. Subsequent analysis in the study aimed at separating the effects of coating roughness from thickness by applying a similar thickness with a smooth coating. This proved that the roughness played a more significant role in deterioration, as the performance reduction in the smooth (but thicker) blade proved to be half that of the rough rotor blade. This finding is also in agreement with Gbadebo et al.[7]

On-wing engine compressor washing is an approach taken to mitigate or eradicate the impact of fouling by the injection of water and/or detergent into the compressor. Figure 3 is a depiction, showing the nozzles placed on the nose cone of the engine. In many existing arrangements, the effluents are not blown to the environment but captured (as shown in Figure 4) and in some cases recycled. Such an activity can be conducted during maintenance check in the hangar or on the airport tarmac after arrival and its frequency is dependent on the maintenance regime and the type of environment for which the aircraft typically operates. The efficiency of these systems has been indicated by a number of airline operators and one of such indicates an annual saving of more

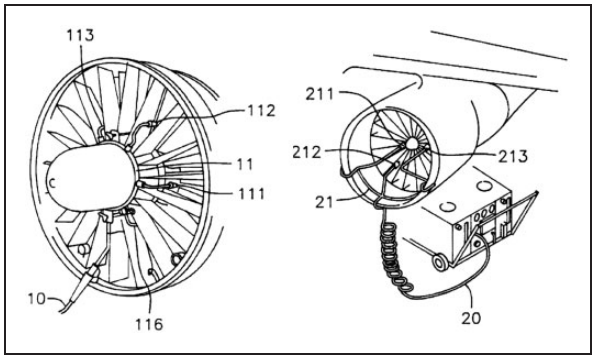

Figure 3. Nozzle arrangements for on-wing washing.[9]

Figure 4. On-wing compressor washing with capture of effluents.[8]

than US$4 million if utilized across their fleet of aircraft.[8] Some of the known benefits of on-wing washing are the improvement of the SFC, thereby reducing exhaust gas temperature (EGT) and extending time on-wing.

The main aim of this study is to evaluate the impact of compressor fouling for a SHM and long-haul mission (LHM), to facilitate the understanding of how their operational requirements and mode of operation influences the severity and impact of compressor fouling.

The engine and aircraft modelling

The performance of the twin-spool turbofan engines has been modelled and simulated using Turbomatch. The Cranfield University in-house program is written in Fortran and it is a zero-dimensional steady-state computer program that simulates the design and off-design performance of most GT configurations using a modified Newton–Raphson method as the convergence technique. This simulation code consists of standard compressor and turbine maps that allows for map scaling and combustion temperature rise chart embedded in the program. Design point calculation is carried out with initial user specification of ambient conditions, pressure losses, component efficiencies, etc. as shown subsequently. Convergence is achieved in the component matching after satisfying compatibility of non-dimensional rotational speed and flow between the compressor and turbine. The off-design compressor and turbine component operating point on their maps are determined based on their calculated scaling factors indicated in equations (1) to (8). An iterative procedure is employed and it involves several trials to ensure that the variables are consistent with the matching constraint (e.g. thrust setting, rotational speed, fuel flow and TET).

The fan and compressors: for off-design calculation, the scaling equations applied to obtain the scaling factors for the compressor is as follows

$$PRSF = \frac{PR_{Dp} - 1}{PR_{Map.Dp} - 1} \tag{1}$$

$$WASF = \frac{WAC_{Dp}}{WAC_{Map.Dp}} \tag{2}$$

$$ETASF = \frac{\eta_C Dp}{\eta_C Map.Dp} \tag{3}$$

Subscript *Dp* is the specified new design point value and *Map.Dp* is the design point value on the standard map. The scaling factors are also used to generate the new compressor maps. For the compressor, the measure of the proximity to the surge line known as the fan/compressor surge margin is also specified and it is defined by the following equation

$$SM = \frac{PR_{Dp} - PR_{HIGH}}{PR_{HIGH} - PR_{LOW}} \times 100 \tag{4}$$

The turbines: for the turbine components driving the compressors, the flow function (also known as the swallowing coefficient) scaling factor is

$$TFSF = \frac{TF_{Dp}}{TF_{Actual}} \tag{5}$$

That of the shaft speed scaling factor is

$$CNSF = \frac{CN_{Dp}}{PCN} \tag{6}$$

PCN is the shaft speed in % and CN is the non-dimensional speed

$$CN = \frac{PCN}{\sqrt{TA}} \tag{7}$$

The scaling factor of the work function is

$$DHSF = \frac{DH_{Dp}}{DH_{Map}} \tag{8}$$

And the turbine efficiency scaling factor is the same formula indicated in equation (3), but relating to the turbine.

The combustor: the combustor efficiency is a plot of combustion efficiency and temperature rise for different constant inlet pressure. This is defined as

$$\eta_{Comb} = \frac{ideal\ amount\ of\ fuel\ burnt}{actual\ amount\ of\ fuel\ burnt} \times 100 \quad (9)$$

Turbomatch models have been validated against commercial data for design and off-design conditions and further details of the programme can be found in MacMillan[10] and Palmer and Pachidis.[11] Walsh and Fletcher[12] also provides details of the working design point and off-design calculations.

The aircraft model implemented is Hermes, another in-house model that accounts for the aerodynamic, structural and loading characteristics of the airframe; all linked with Turbomatch and hence enables the calculation of thrust settings and engine performance for the different flight segments and deviation mission.[13] Hermes is based on aircraft performance theory explained in Jenkinson et al.[14] The software consists of six modules as illustrated in Figure 5, which also shows the interactions of these modules. The input data module includes the geometric characteristics such as the span, swept angle, wing area, tip-to-chord ratio, fuselage length and diameter that enables the estimation of aircraft drag and performance.[15] The parameters in this module are used in the aerodynamic and aircraft performance modules to estimate the aerodynamic performance and performance of the aircraft respectively. The mission profile module includes the user specification of the mission profile: taxi, take-off, climb, cruise and descent schedules as well as their respective altitudes. This information is subsequently used for computing time, distance and fuel consumption. For the atmospheric module, ISA is assumed and the corresponding static temperature and pressure are calculated for the given altitude and the Mach number. It also allows for deviations in ISA, which is easily adapted using polynomials that includes the specific heat ratio and specific heat capacity of air and other gases related to temperature. The engine performance module includes the outcome of the simulation of Turbomatch at design and off-design conditions. The engine performance includes the maximum take-off thrust (MTOT), maximum climb thrust and SFC, cruise and descent performance.

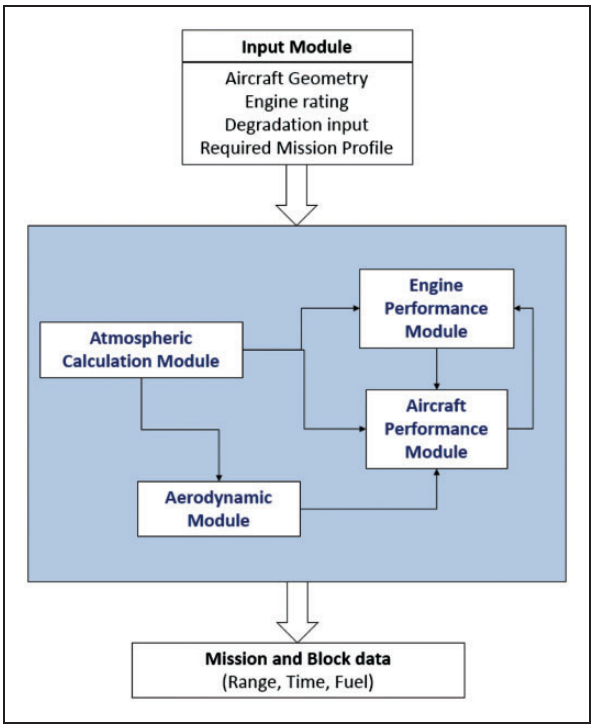

Figure 5. Illustration showing the different HERMES modules and their interactions.

The calculation of the drag characteristics of the aircraft is computed in form of zero-lift and lift-induced coefficients, using the component build-up method.[16,17] This is performed in the aerodynamic module taking into account information from the input data, mission profile and atmospheric modules. Further explanation is presented in Hanumanthan et al.[15] To calculate the total drag coefficient, it is the sum of the zero lift drag coefficient (lift dependent) and the induced drag coefficient (lift independent) as follows

$$C_D = C_{D0} + C_{Di} \quad (10)$$

The zero lift drag coefficient for the fuselage or wing can fully be expressed in the following equation

$$C_{D0} = \frac{\sum \left(Cf_c, \varphi_c, Q_c, S_{c,w}\right)}{S_{ref}} \quad (11)$$

were Cf_c is the skin friction coefficient, φ_c is the form factor for estimating subsonic profile drag, Q_c accounts for the interference drag, $S_{c,w}$ is the wetted surface area and S_{ref} is the plan form area. Hence, the overall C_{D0} is the sum of the respective aircraft component zero lift drag divided by the plan form area. For the induced drag coefficient, the mathematical expression is

$$C_{Di} = \left[\left(\frac{C_1}{C_2 \times \mu \times AR}\right) + C_3 + C_4 \times C_{D0}\right] \times C_L^2 \quad (12)$$

C_1 and C_2 are coefficients to account for the wing plan form geometry and are functions of the wing aspect ratio AR, while C_3 and C_4 are coefficients to account for the non-optimum wing twist and viscous effects, respectively and C_L is the lift coefficient. To estimate the aerodynamic efficiency, it is the lift-to-drag ratio as indicated in the following equation. For the cruise condition with constant aircraft speed V, the

aerodynamic drag is equal to the thrust.

$$A_e = \frac{0.5 \times \rho \times C_L \times V^2 \times S_{ref}}{0.5 \times \rho \times C_D \times V^2 \times S_{ref}} = \frac{C_L}{C_D} \quad (13)$$

For the aircraft performance module the output is the fuel consumed, distance covered, duration of mission, engine thrust and SFC for each segment of the mission and as a whole performance for every segment of the mission. The total fuel consumed is the integral of the fuel flow indicated in the following equation

$$M_f = \int_{t1}^{t2} SFC \times F_N \mathrm{d}t \quad (14)$$

The time required to fly from altitude a_1 to a_2 is solved by the following

$$t_i = \int_{a_2}^{a_1} \frac{1}{V_{vert}} \mathrm{d}h \quad (15)$$

where V_{vert} is the vertical velocity and the rate of climb expressed as

$$V_{vert} = \frac{\mathrm{d}h}{\mathrm{d}t} \quad (16)$$

The other mathematical expression for calculating the total time of flight, total distance covered by the aircraft and key aircraft performance calculations applicable to HERMES software is available in Laskaridis et al.[16]

Airframe and engine model specifications and missions

The airframes considered are based on the Embraer EMB 145 and Airbus A330-200 type specifications for the SHM and LHM, respectively. This short-haul aircraft has a capacity of 50 passengers and a maximum range under maximum load of 1500 NM (nautical miles). For the LHM the passenger capacity is around 300, with a range of 7200 NM. Table 1 indicates the airframe specification implemented for both aircraft models, while Table 2 shows the aircraft operational requirements and defined limits in the model which compare to the manufacturer's specification in Jenkinson et al.[14] and Jackson[18] for these aircraft.

The engine models considered are both two spool, powered by Rolls Royce AE3007 type engine for the SHM and the General Electric CF6-80E1A2 type for the LHM as exists in practice. Their specifications as indicated are inspired by the manufacture's specification available in public domain. Figure 6 depicts the design of the engine, consisting of two spools. As shown in this configuration, the fan and booster compressor are on the same shaft and hence have the same rotational speed. The HP spool 'sees' a lower non-dimensional mass flow due to higher inlet temperatures and operates at a higher rotational speed to achieve a higher pressure ratio. As would be observed in Table 3 the LHM aircraft has a cruise thrust (design point) about 7 times the SHM aircraft. The take-off thrust is about 5 times greater than the cruise thrust for both aircraft respectively as shown in Figures 7 and 10. The SFC at design point is similar for both engines as shown in the table. The specified compressor and turbine efficiencies for the LHM engine has been specified to be a little better than the other engine due to higher pressure ratio, mass flow and thrust necessary for this bigger engine and as a such the specified TET is higher. It is important to state that the TET during take-off is a lot higher as shown in the latter part of this paper. Values of TET in this condition can reach 1700 K for modern advanced engines.[19]

The mission profiles for the short- and long-haul flights are presented subsequently and Table 4 indicates the period of each segments of the flight in minutes, as well as the their respective proportion relative to the overall flight time (%). What can be observed is that the take-off period for both flights is just 3 minutes difference; however the take of period constitutes only 3% of the overall mission for the LHM, compared to the SHM which is about 12%. The climb and

Table 1. Airframe model specifications.

Parameters	SHM Model EMB 145	LHM Model A330-200
Overall length (m)	27.9	57.8
Fuselage diameter (m)	2.3	5.6
Wing area (m^2)	51.2	363.1
Wing aspect ratio (–)	7.9	9.3
Tailplane area (m^2)	11.2	31.0
Tailplane AR (–)	5.2	5.0

SHM: short-haul mission; LHM: long-haul mission.

Table 2. Aircraft requirements and defined limits.

Haul/Flight	SHM	LHM
Maximum take-off weight (MTOW) (kg)	22,000	230,000
Maximum payload weight (MPW) (kg)	5786	49,000
Fuel for maximum payload weight (kg)	4614	61,700
Maximum zero-fuel weight (MZFW) (kg)	17,386	168,000
Operating empty weight (OEW) (kg)	11,600	120,200
Range at maximum payload (Nm)	1500	7200
Number of passenger seating	50	300
Number of engines	2	2

SHM: short-haul mission; LHM: long-haul mission.

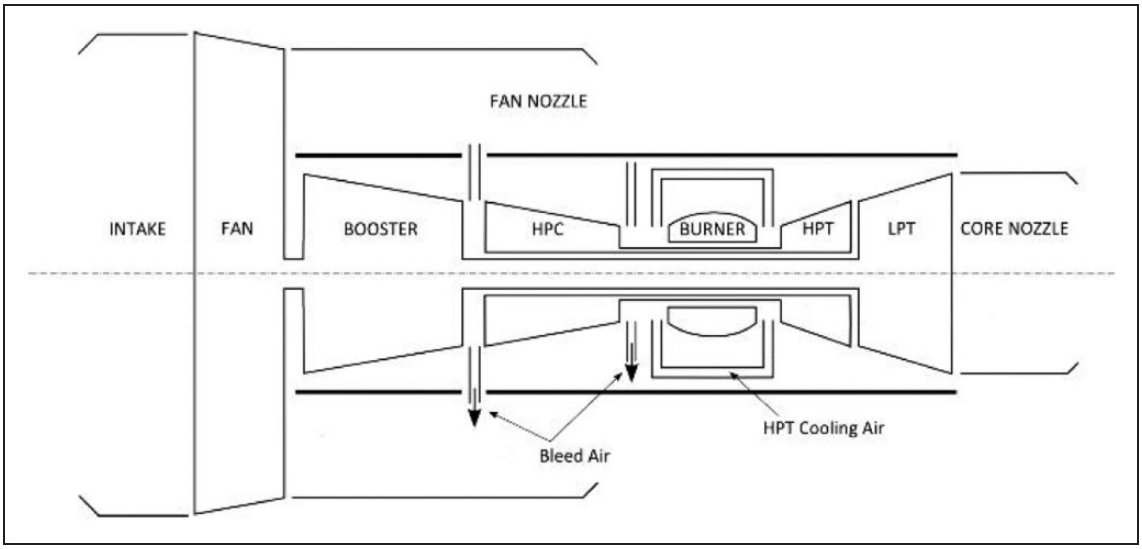

Figure 6. Two-spool gas turbine configuration.[3]

Table 3. Design point specifications of engine models.

Design point of engine models – Cruise - ISA		
Mach number: $Ma = 0.8$,		
Altitude = 10,886 m		
Haul/Flight	SHM	LHM
Net thrust (kN)	7.4	53.3
Mass flow (kg/s)	57.7	355.0
Bypass ratio (–)	4.9	5.2
Overall pressure ratio (OPR) (–)	24.9	33.3
Fan pressure ratio (–)	1.6	1.8
Booster pressure ratio (–)	2.7	2.9
HPC pressure ratio (–)	5.9	6.4
Fan efficiency (%)	86.0	88.0
Booster compressor efficiency (%)	87.0	88.5
HPC efficiency (%)	87.0	87.5
HPT cooling flow (%)	10.0	11.0
Combustor efficiency (%)	99.0	96.0
Combustor pressure loss (%)	6.0	4.0
SFC (g/(kN*s))	17.5	17.0
Turbine entry temperature (K)	1230	1370
HPT efficiency (%)	90.0	92.0
LPT efficiency (%)	91.0	93.0

ISA: international standard atmosphere; HPC: high-pressure compressor; HPT: high-pressure turbine; SFC: specific fuel consumption; LPT: low-pressure turbine.

descent segments are also a greater proportion in the SHM with the exception of cruise segments. The cruise segment in the LHM is about 14 times the SHM. The influence on theses operational factors is also presented and discussed in the later part of this paper.

Flight and performance simulation

The outcome of the simulation of the SHM is presented in Figure 7 for the clean engine. This shows the flight or mission profile, with maximum altitude of 10,668 m (35,000 feet). For various segments of the flight it would be observed that the thrust settings vary. The maximum thrust throughout the mission is reached at take-off. In this condition higher rotational shaft speed is attained, leading to higher mass flow and fuel flow. This consequently increases the turbine entry temperature (TET) and EGT as shown in Figure 8 which indicates the highest TET and EGT at take-off operation. Figure 7 also shows a gradual reducing thrust setting from climb to cruise segment. This is as a result of the reducing air density and drag on the aircraft with increasing altitude. In the climb phase the aircraft is controlled to ascend at a desired rate of climb (ROC) and calibrated air speed (CAS) and hence the engine is operated at the max climb rating. This constitutes a power setting which is lower than that maintained at take-off, but higher than set for the cruise phase of the flight. During climb, it can be observed that the constant high value for the TET is maintained irrespective of the reducing thrust reduction. This is attributed to the reducing mass flow penalty due to reduced density, in combination with power setting (including rotational speed) reduction. This causes an increase SFC as shown in Figure 9.

At cruise the thrust required will be such that whilst maintaining altitude, the drag effects are cancelled by the engine's thrust. Therefore, the power setting of the GT at the beginning of the cruising phase will be considerably lower than that associated to top of climb. Another observation is that the TET progressively drops during the cruise phase; however, this is not obvious in Figure 8, unlike that of the LHM due

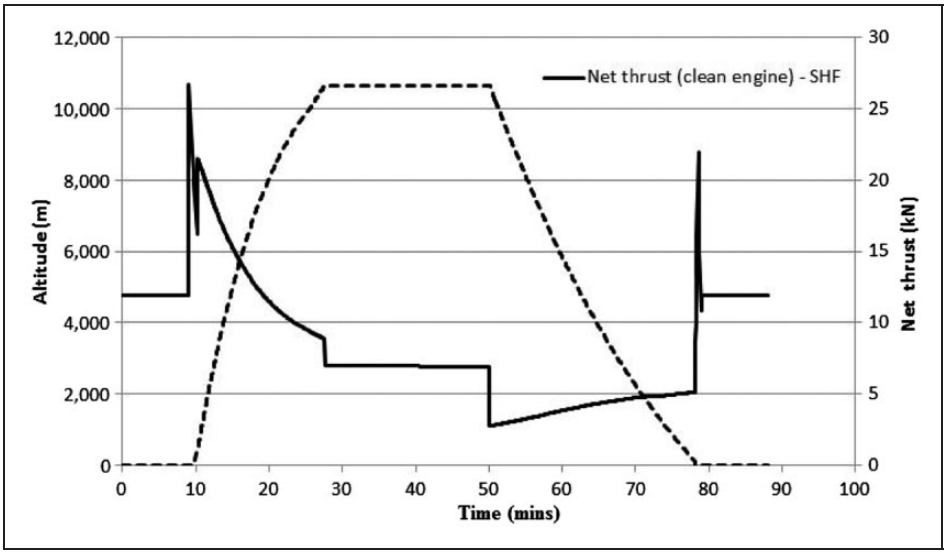

Figure 7. Change in altitude /mission profile and net thrust with time – SHM.

Table 4. Period of flight segments for the SHM and LHM.

Flight segments	SHM	LHM
Taxi to take-off (min)	10.3	13.6
Time to take-off (%)	11.7	3.3
Climb period (min)	17.3	17.1
Period of climb (%)	19.7	4.1
Cruise period (min)	22.4	316.1
Period of cruise (%)	25.5	76.6
Descent period and landing (min)	37.9	66.2
Period of descent and landing (%)	43.1	16.0
Overall flight time (min)	87.9	412.9

SHM: short-haul mission; LHM: long-haul mission.

to the longer period of cruise. The slight reduction is mainly due to the gradual reduction of aircraft weight and hence thrust with time. During the descent phase the operating condition changes, as the aircraft operates with increasing effect of gravity, higher density and mass flow with reduction in altitude. As a result the engine is operated at relatively lower settings compared to the earlier segments of the flight. Figure 7 shows a small and gradual increase in net thrust from the period of descent notwithstanding, due to the modulation of variable stator vane (VSV) angles to maintain TET as shown in Figure 8. The consequence here is an increase in SFC as shown in Figure 9. The VSV opening is reduced to accommodate for the increasing mass flow with reduced height, nevertheless in this model the new angle is fixed throughout descent and not variable. As a result there is a small increase in thrust. As the aircraft touches ground the net thrust, TET and EGT peaks due to the deployment of the thrust reverser causing the SFC to drop.

For the LHM the same maximum altitude is reached as shown in Figure 10. This shows similar patterns with the SHM except for the fact that the cruise period is longer. Figure 11 shows a more obvious decrease in TET from start to end of cruise. In addition to this, it can be observed that the operating TET and EGT are generally higher than engine for the SHM. The maximum TET and EGT in comparison to the SHM is +290 K and +81 K, respectively. This is due to higher thrust and payload when compared to the smaller engine for the SHM. Figure 12 shows the SFC trend for the LHM that is comparable to the SHM.

Compressor fouling cases and effects

The cases of compressor fouling investigated are indicated in Table 5. Igie et al.[1] shows that the impact of fouling is the alteration of the aerodynamic shape of the compressor blade, increases in surface roughness and reduction in the blade effective flow passage. This effect is characterised by implanting a flow capacity reduction (related to additional materials on the blade, as well as increased boundary layer) and a reduction of compressor efficiency (related to induced drag caused by roughened surface and change in blade geometry). It is important to state that fouling levels on aircraft engines are difficult to measure in these terms due to lack of such instrumentations in most aero engines as already stated and due to intrusive methods for such level of details, including concern about weight. However the operating temperatures that can include the compressor discharge temperature (CDT), ITT and EGT are typically used to evaluate deviations from the expected normal conditions. Three fouling cases have been investigated; from a lower level (case 1) up to a higher level of degradation (case 3) to observe the corresponding impacts on performance, especially TET and fuel burn for this range of

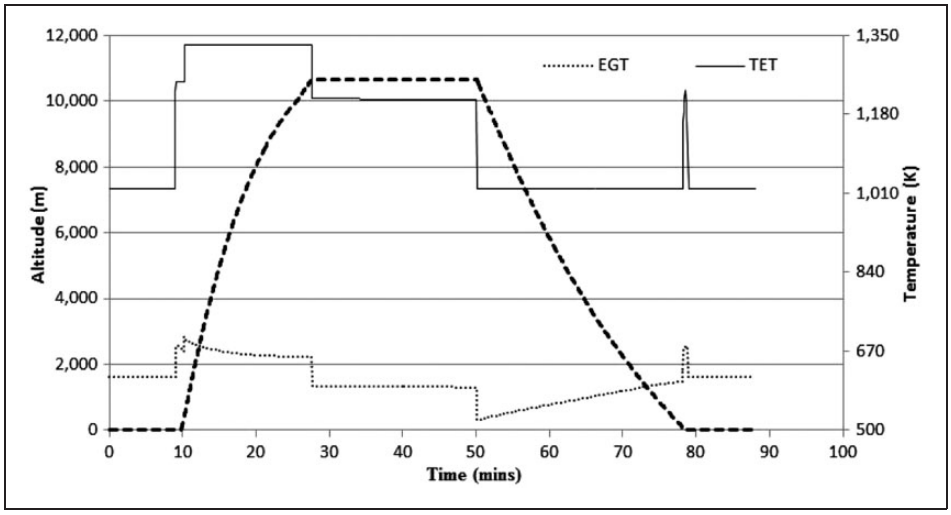

Figure 8. TET and EGT during the mission – SHM.

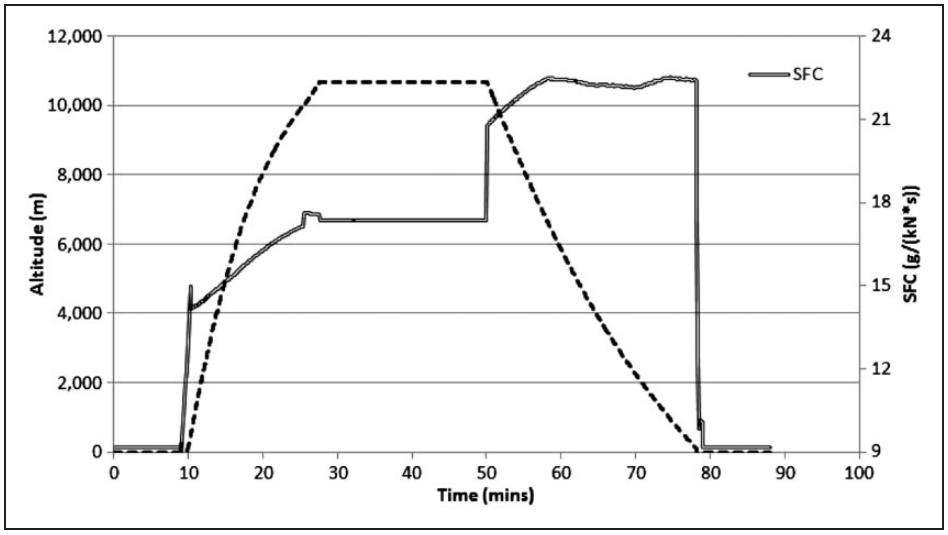

Figure 9. SFC during the mission – SHM.

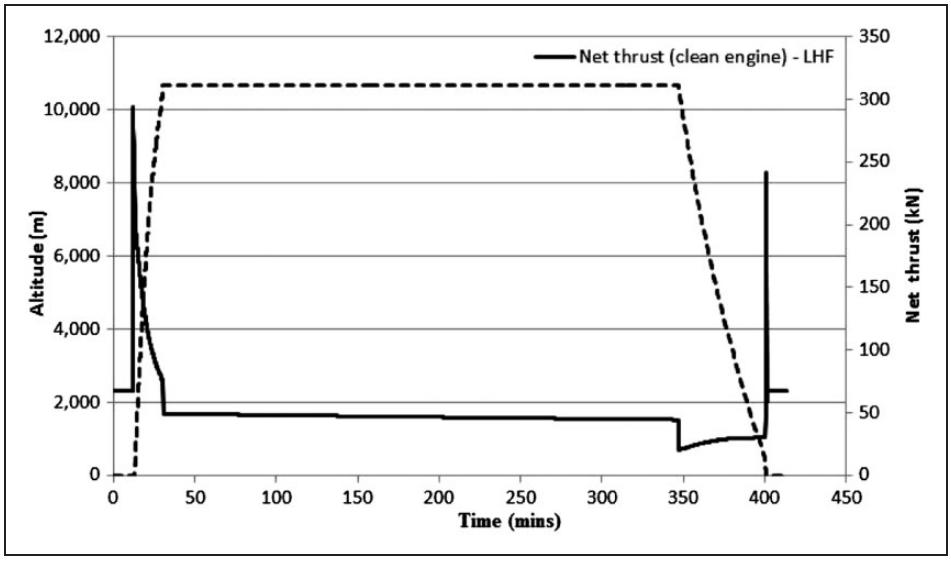

Figure 10. Change in altitude /mission profile and net thrust with time – LHM.

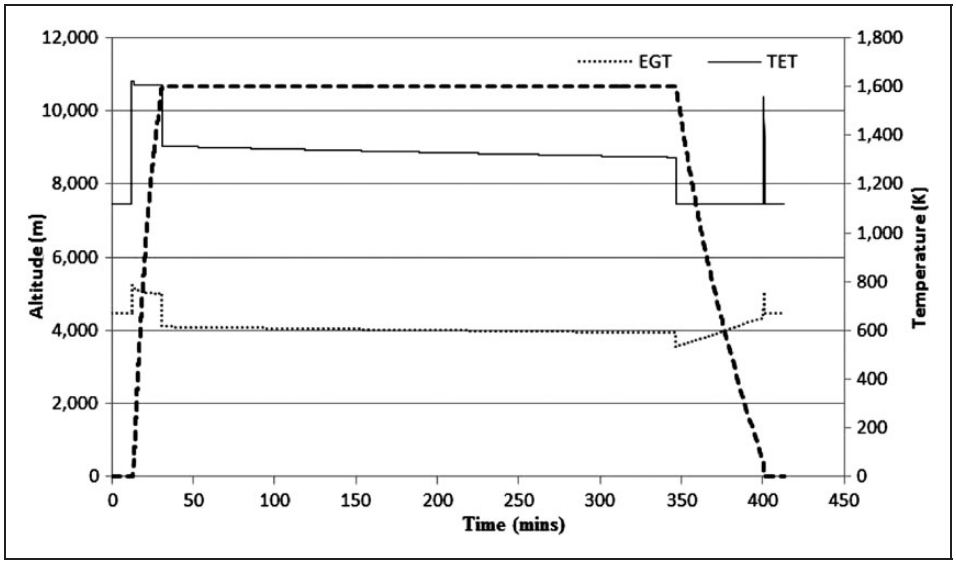

Figure 11. TET and EGT during the mission – LHM.

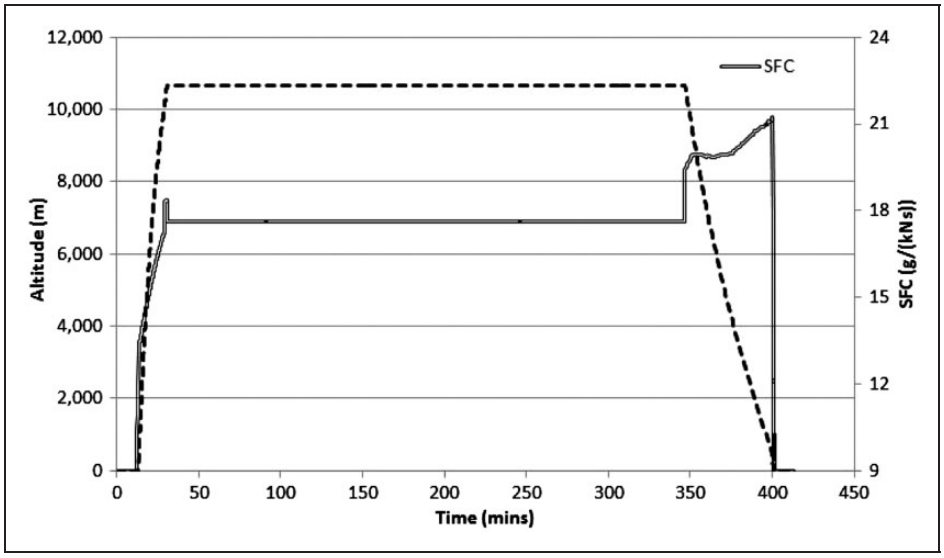

Figure 12. SFC during the mission – LHM.

Table 5. Compressor fan degradation cases.

Cases	Flow capacity reduction (%)	Fan compressor efficiency reduction (%)
Case 1	1	1
Case 2	3	1
Case 3	5	2

degradation levels. Simply attributing any one of these cases as a function of time or number of flight cycles in actual operation is not possible as it is also dependent on the environment for which the aircraft flies, thrust settings which are also influenced by the payload. In most fouling studies, it would be observed that the flow capacity reduction is greater than the compressor efficiency reduction. The opposite is the case when fouling occurs in the back stage and not the front stage as demonstrated in Igie et al.[1] and Millsaps et al.[20] for single-spool compressors. An example of this occurrence is a washed compressor for which foulants in the front stages are re-deposited in the back stages. This possibility is demonstrated in Syverud and Bakken.[21]

For this study, only the fan is assumed to be fouled as studies in open literature show that the front blades are the most fouled and also proven in Syverud et al.[4]

The impact of these degradations on the SHM engine is presented in Figures 13 and 14 which show the changes in TET and SFC (%) for the respective cases. Throughout the mission, it is observed that the engine runs hotter relative to the clean engine as shown in Figure 13. For the mission, it can be observed that the highest penalty is during take-off

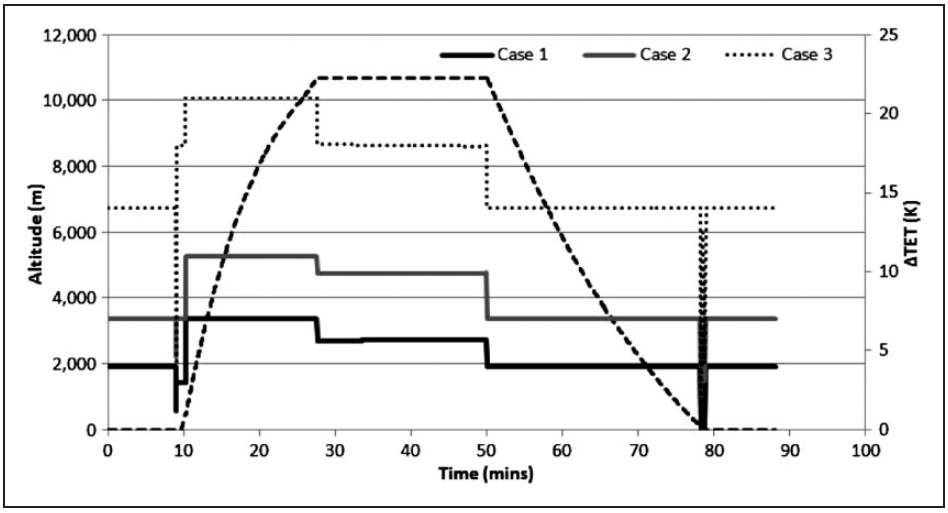

Figure 13. Change in TET due to fouling – SHM.

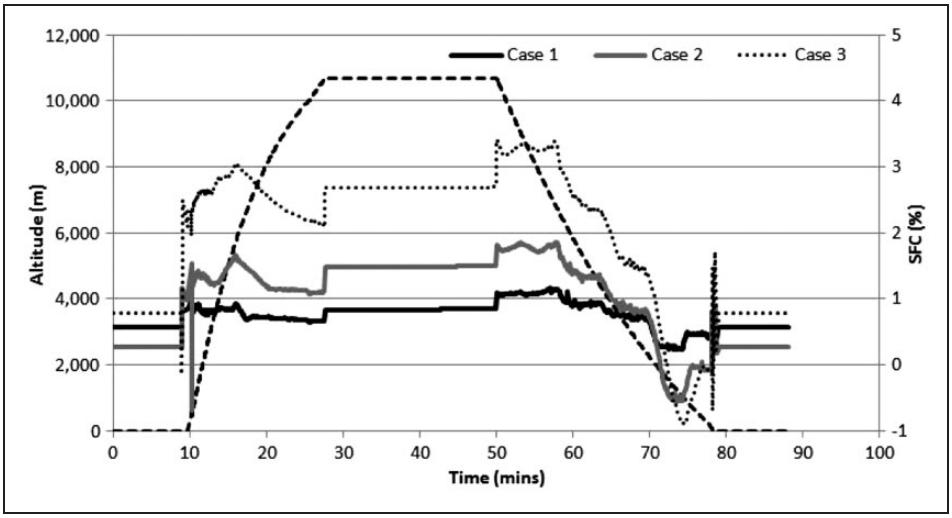

Figure 14. Change in SFC due to fouling – SHM.

and climb segments due to the relatively higher thrust setting as shown in Figure 7. There are step reductions in the penalty from cruise and also descent phase following thrust reductions. Case 3 shows the highest temperature rise as expected and its take-off temperature rise is about 21 K. It is in fact a rise of about 7 K, 11 K and 21 K respectively + 1330 K at take-off for the respective degradations. The increase in temperature is a result of increase in fuel burn, to attain similar thrust as the normal clean condition. This also translates to increase in EGT and emissions. The change in SFC for the SHM is indicated in Figure 14 showing higher fuel consumption with increase in fouling levels.

Similar changes can be observed for the LHM as shown in Figures 15 and 16. For the LHM the rise in TET due to fouling is 7 K, 10 K and 17 K respectively + 1620 K. An observation from both missions based on temperature rise indicates that for the lowest fouling cases 1 and 2, the penalties are similar but slightly worse for the short-haul engine by only 4 K for the worst degradation (case 3).

The additional fuel burn for both missions for their respective cases of degradation is presented in Table 6 (for one engine per aircraft). This shows that in the most severe degradation (case 3) the penalty on the SHM is greater than the LHM by only 0.8% points more in increase in fuel burn. This is not significant but can be attributed to the relatively longer period of take-off segment in the SHM. However, it can be observed again that this relatively minimal impact is almost negligible at lower fouling levels.

Conclusions

The investigation shows some of the impacts of compressor fouling on the two-spool engine models for SHM and LHM for assumed levels of degradation (from low to very high). It was observed that for the SHM, despite take-off/climb segment constituting a

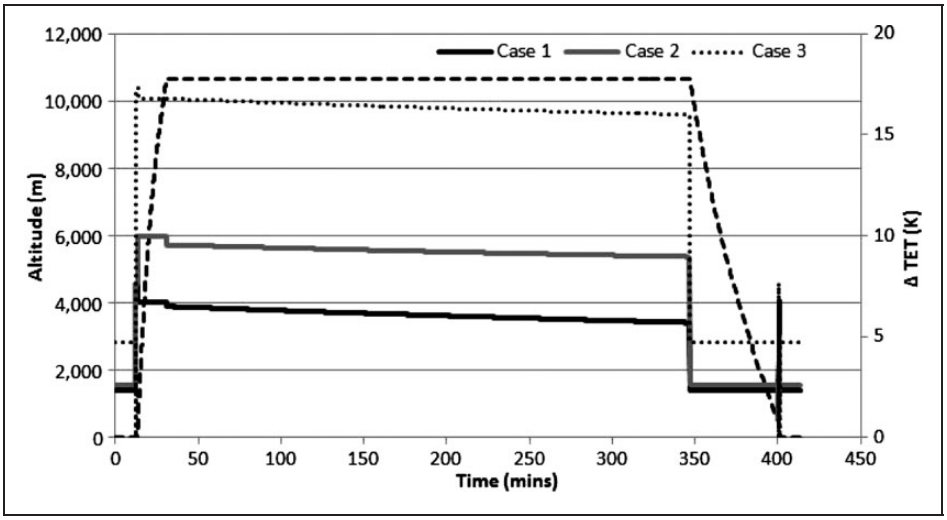

Figure 15. Change in TET due to fouling – LHM.

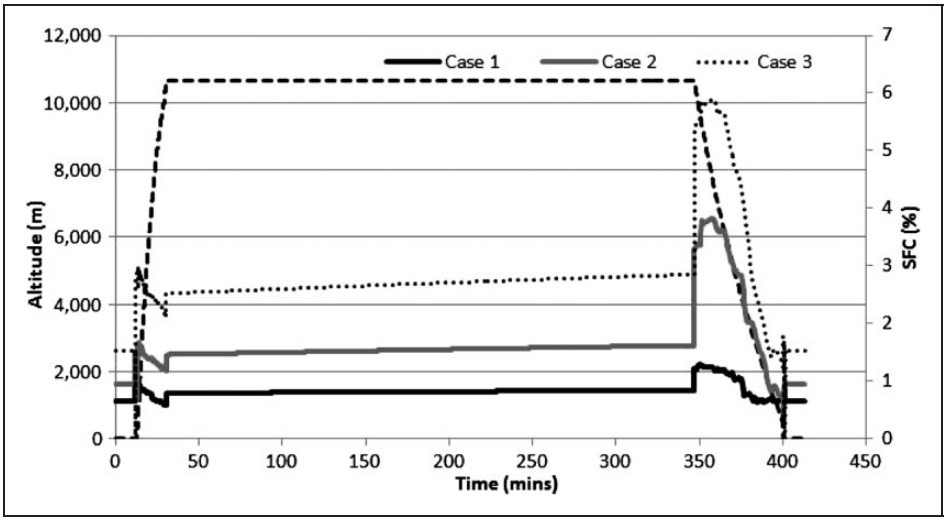

Figure 16. Change in SFC due to fouling – LHM.

Table 6. Additional fuel burn due to fouling per engine for SHM and LHM.

Missions	Clean	Case 1	Case 2	Case 3
SHM	1175 kg	+11 kg (0.9%)	+21 kg (1.8%)	+42 kg (3.6%)
LHM	39,138 kg	+344 kg (0.9%)	+611 kg (1.6%)	+1097 kg (2.8%)

SHM: short-haul mission; LHM: long-haul mission.

larger proportion in the overall mission compared to the LHM, the penalty due to fouling is the same except for higher levels were the impact is minimally higher. It is important to state however in practice, such high level of degradation would not usually be reached before an on-wing wash. The least case of fouling shows a temperature rise of 7 K for both engines for their various missions during take-off. This is significant given that for some turbine technology, the life of the blades can be halved by 10 K rise in temperature. The extent of this would be defined by the cooling and materials employed, as well as whether the engine is operating closer to its maximum flat rating or derated. The added fuel burn during fouling in relation to fuel cost of US$0.5/kg indicate very little penalty on additional fuel cost when compared to the potential non-recoverable turbine loss, life reduction and downtime associated with high temperature rise.

Taking into account that in practice the SHM engine would typically run more flight cycles than the LHM for the same period of time, larger EGT

margins alongside derate thrust settings can help mitigate the impact of fouling on the life of the turbine blades. It is also important to state that fouling is an accumulative process and the lower fouling cases simulated would accrue over a long period of time; all determined by the nature of the environments and frequency of on-wing washing. In addition, it is very unlikely that case 3 investigated here would be allowed in operation. The inclusion in this study is to make the point that in the extreme case, fuel burn due to fouling degradation is still less important than the rise in turbine blade temperature.

Conflict of interest

The authors declared no potential conflicts of interest with respect to the research, authorship, and/or publication of this article.

Funding

The authors received no financial support for the research, authorship, and/or publication of this article.

References

1. Igie U, Pilidis P, Fouflias D, et al. Industrial gas turbine performance: Compressor fouling and on-line washing. *J Turbomach* 2014; 136: 101001-101001.
2. Alpert P, Kishcha P, Shtivelman A, et al. Vertical distribution of Saharan dust based on 2.5-year model predictions. *Atmos Res* 2004; 70: 109–130.
3. Giesecke D, Igie U, Pilidis P, et al. Performance and techno-economic investigation of on-wing compressor wash for a short-range aero engine. In: *ASME turbo expo 2012*, Copenhagen, 11 June 2012, pp.235–244.
4. Syverud E, Brekke O and Bakken LE. Axial compressor deterioration caused by saltwater ingestion. *J Turbomach* 2007; 129: 119–126.
5. Tarabrin AP, Bodrov AI, Schurovsky VA, et al. Influence of axial compressor fouling on gas turbine unit performance based on different schemes and with different initial parameters. In: *ASME international gas turbine and aeroengine congress*, Stockholm, Sweden, 1998, ASME paper no. 98-GT-416.
6. Suder KL, Chima RV, Strazisar AJ, et al. The effect of adding roughness and thickness to a transonic axial compressor rotor. *J Turbomach* 1995; 117: 491–505.
7. Gbadebo SA, Hynes TP and Cumpsty NA. Influence of surface roughness on three-dimensional separation in axial compressors. *J Turbomach* 2004; 126: 455–463.
8. AviationPros. ASIG signs exclusive engine wash deal from GE aviation. AviationPros.com. http://www.aviationpros.com/press_release/10709699/asig-signs-exclusive-engine-wash-deal (accessed 11 July 2014).
9. Asplund P. Spraying with finely divided liquid. US5868860 A, February 1999.
10. MacMillan W. *Development of a modular type computer program for the calculation of gas turbine off design performance*. PhD Thesis, Cranfield University, Cranfield, UK, 1974.
11. Palmer JR and Pachidis V. The turbomatch scheme; for aero/industrial gas turbine engine design point/off design performance calculation. Cranfield University, Cranfield, UK, 2005.
12. Walsh PP and Fletcher P. *Gas turbine performance*. Malden, MA: Blackwell Science, 2004.
13. Doulgeris G, Korakianitis T, Avital EJ, et al. Effect of jet noise reduction on gas turbine engine efficiency. *Proc IMechE, Part G: J Aerospace Engineering* 2012; 0954410012456925.
14. Jenkinson LR, Rhodes D and Simpkin P. *Civil jet aircraft design*. London: Arnold, 1999, p.436.
15. Hanumanthan H, Stitt A, Laskaridis P, et al. Severity estimation and effect of operational parameters for civil aircraft jet engines. *Proc IMechE, Part G: J Aerospace Engineering* 2012; 226: 1544–1561.
16. Laskaridis P, Pilidis P and Kotsiopoulos P. An integrated engine-aircraft performance platform for assessing new technologies in aeronautics. In: *Proceedings of the 17th international symposium on air breathing engines*, Munich, Germany, 2005.
17. Torenbeek E. *Synthesis of subsonic airplane design: An introduction to the preliminary design of subsonic general aviation and transport aircraft, with emphasis on design, propulsion and performance*. Delft: The Hague, 1982Hingham, MA: Springer, 1982, 624 pp.
18. Jackson PA. *Jane's all the world's aircraft 2012/2013: Development & production*. 103rd ed. Coulsdon: Jane's Information Group, 2012, p.1032.
19. Han J-C, Dutta S and Ekkad S. *Gas turbine heat transfer and cooling technology*. 2nd ed. Boca Raton: CRC Press, 2012, p.891.
20. Millsaps KT, Baker J and Patterson JS. Detection and localization of fouling in a gas turbine compressor from aerothermodynamic measurements. In: *Conference: ASME turbo expo 2004: power for land, sea, and air*, 2004, pp.1867–1876.
21. Syverud E and Bakken LE. Online water wash tests of GE J85-13. *J Turbomach* 2007; 129: 136–142.

Appendix

Notation

a_1	start altitude (m)
a_2	final altitude (m)
A_e	aerodynamic efficiency
AR	aspect ratio
C_D	total drag coefficient
C_{D0}	zero lift drag coefficient (lift dependent)
C_{Di}	induced drag coefficient (lift independent)
C_{fc}	skin friction coefficient
C_L	lift coefficient
C_1	coefficient to account for the wing plan form geometry
C_2	coefficient to account for the wing plan form geometry
C_3	coefficient to account for the non-optimum wing twist
C_4	coefficient to account for viscous effects twist
CN	non-dimensional shaft speed relative to design

$CNSF$	scaling factor for non-dimensional shaft speed
DH	turbine work function
$DHSF$	scaling factor of the work function
$ETASF$	isentropic efficiency scaling factor
F_N	thrust (kN)
Ma	Mach number
M_f	total fuel consumed (kg)
PCN	shaft rotational speed as a percentage of design point (%)
PR	pressure ratio
PR_{HIGH}	highest pressure ratio for a given constant speed line at surge
PR_{LOW}	lowest pressure ratio for a given constant speed line at choke
$PRSF$	pressure ratio scaling factor
Q_c	parameter accounts for the interference drag
$S_{c,w}$	wetted surface area
S_{ref}	plan form area
SM	surge margin (%)
t_1	start time (min)
t_2	end time (min)
TA	ambient temperature (K)
TF	turbine flow function or swallowing coefficient
$TFSF$	scaling factor for turbine flow function using turbine map
V	velocity (m/s)
WAC	non-dimensional mass flow
$WASF$	mass flow scaling factor
μ	dynamic viscosity
ρ	density
η_C	compressor isentropic efficiency
η_{Comb}	combustor efficiency
φ_c	form factor for estimating subsonic profile drag

Subscripts

$Actual$	value of quantity obtained from actual component conditions as opposed to map value
D_p	design point conditions
$Map_{.Dp}$	value of design parameter obtained from component map
$vert$	vertical